Biophysical Journal
Article

Biophysical Society

Mechanisms of Light-Induced Deformations in Photoreceptors

K. C. Boyle,[1,2,*] Z. C. Chen,[1,2] T. Ling,[2,3] V. P. Pandiyan,[4] J. Kuchenbecker,[4] R. Sabesan,[4,*] and D. Palanker[2,3,*]
[1]Department of Electrical Engineering, [2]Hansen Experimental Physics Laboratory, and [3]Department of Ophthalmology, Stanford University, Stanford, California; and [4]Department of Ophthalmology, University of Washington, Seattle, Washington

ABSTRACT Biological cells deform on a nanometer scale when their transmembrane voltage changes, an effect that has been visualized during the action potential using quantitative phase imaging. Similar changes in the optical path length have been observed in photoreceptor outer segments after a flash stimulus via phase-resolved optical coherence tomography. These optoretinograms reveal a fast, millisecond-scale contraction of the outer segments by tens of nanometers, followed by a slow (hundreds of milliseconds) elongation reaching hundreds of nanometers. Ultrafast measurements of the contractile response using line-field phase-resolved optical coherence tomography show a logarithmic increase in amplitude and a decreasing time to peak with increasing stimulus intensity. We present a model that relates the early receptor potential to these deformations based on the voltage-dependent membrane tension—the mechanism observed earlier in neurons and other electrogenic cells. The early receptor potential is caused by conformational changes in opsins after photoisomerization, resulting in the fractional shift of the charge across the disk membrane. Lateral repulsion of the ions on both sides of the membrane affects its surface tension and leads to its lateral expansion. Because the volume of the disks does not change on a millisecond timescale, their lateral expansion leads to an axial contraction of the outer segment. With increasing stimulus intensity and the resulting tension, the area expansion coefficient of the disk membrane also increases as thermally induced fluctuations are pulled flat, resisting further expansion. This leads to the logarithmic saturation observed in measurements as well as the peak shift in time. This imaging technique therefore relates the structural changes in the photoreceptor to the underlying neurological function of transducing light into electrical signals. Such label-free optical monitoring of neural activity using fast interferometry may be applicable not only to optoretinography but also to neuroscience in general.

SIGNIFICANCE Nanometer-scale cellular deformations have been observed in cells during the action potential. We demonstrate such changes in the optical path length in photoreceptors after a light stimulus in vivo using phase-resolved optical coherence tomography. We present a model that relates electrical activity during phototransduction to deformations based on the voltage-dependent membrane tension—the mechanism observed earlier in neurons and other electrogenic cells. The model closely matches measurements in human photoreceptors, indicating that it is generally applicable to all electrogenic cells regardless of the underlying mechanism of the transmembrane potential or cell morphology. Label-free optical monitoring of neural activity in vivo relates function to structure and should greatly improve our functional imaging capabilities in neuroscience in general and in ophthalmology in particular.

INTRODUCTION

Retinal photoreceptors convert light into electrical signals through a phototransduction cycle that operates across multiple timescales from milliseconds to seconds. Understanding the resulting electrical and biochemical activity throughout this response is very important for comprehending visual function in general and for diagnosis of its pathology in particular. Until now, electrical signals in photoreceptors and other retinal cells have been measured using intracellular or extracellular electrodes (1–3). Recently, phase-resolved imaging of photoreceptors demonstrated significant changes in the optical path length (OPL) in response to flash stimuli (4–6). Similarly, nanometer-scale OPL changes accompanying the action potential have been observed in spiking neurons ex vivo and have been shown to faithfully reproduce changes in the cell potential (7–9).

Submitted March 20, 2020, and accepted for publication September 8, 2020.
*Correspondence: kcb76@stanford.edu or rsabesan@uw.edu or palanker@stanford.edu
Editor: Michael Brown.
https://doi.org/10.1016/j.bpj.2020.09.005

Interferometric imaging of such nanometer-scale changes over millisecond timescales offers a noninvasive and label-free alternative to current electrophysiological methods, which may allow in vivo studies of neurobiology, especially retinal physiology.

To relate the observed mechanical deformations of cells to the underlying physiological processes, the coupling mechanisms must be known. Recently, we demonstrated that nanometer-scale deformations in neurons and other electrogenic cells can be explained by the voltage dependence of the membrane tension (8,10). Changes in the membrane tension cause a deformation to rebalance forces across the structure, whether it is a whole cell or an organelle. The charged membranes in photoreceptors are no exception and should similarly link electrical activity to deformations.

Here, we study the mechanisms underlying the changes in photoreceptor outer segments after brief stimuli, such as observed in human eyes, using phase-resolved optical coherence tomography (pOCT). We present a model of the light-induced deformation that fits the measured data across multiple stimulus intensities and discuss how such a model can aid in characterizing the phototransduction cycle or the mechanical properties of the disk membranes. We also discuss how the model can help enhance the sensitivity of future recordings.

MATERIALS AND METHODS

To capture the dynamics of the fast response and allow exploration of the underlying mechanism, we used a line-scan pOCT system, which is shown in Fig. S1 *a*. This is an interferometric imaging system that captures the relative OPL in a sample arm aligned with a subject's retina to a static reference arm. It enables sub-millisecond time resolution of axial deformations across a field of view containing tens of photoreceptors. This system is described in detail in (11,12), in which recordings made in the living human eye via pOCT demonstrated significant OPL changes in the outer segments of photoreceptors in response to light stimuli, as shown in Fig. 1. The photoreceptor response begins with a fast, millisecond-scale contraction by a few tens of nanometers, followed by a much slower (hundreds of milliseconds) and much larger (hundreds of nanometers) elongation (11,13).

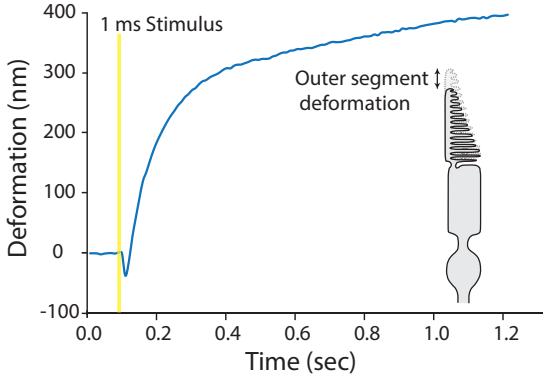

FIGURE 1 OPL changes in the photoreceptor outer segment in response to light stimuli. A brief flash (in this case 1 ms at 6.11×10^6 ph/μm^2) elicits a fast, millisecond-scale contraction (negative deformation), which is then overtaken by a hundreds-of-milliseconds-long elongation. To see this figure in color, go online.

These deformations were induced by the light stimulus projected in a three-bar pattern across the field of view and recorded using the pOCT system. The resulting changes, synchronized to the onset of the light stimulus, occurred only in photoreceptors within the structured light pattern, as shown in Fig. S1 *b*. An additional control experiment in Fig. S1 *c* shows no response over time from photoreceptors without a stimulus compared with the deformation signal measured in stimulated photoreceptors.

To assess a potential thermal effect of the stimulus, we estimated the corresponding temperature rise using the finite element of the retina, as described in our previous work (14). For the 1 ms stimulus at 3.6×10^6 photons/μm^2 intensity, the temperature rise in the photoreceptor outer segment does not exceed 5 mK. The corresponding linear thermal expansion would be <0.015 nm, assuming a high-end linear expansion coefficient of 3×10^{-4} K^{-1}, which is about a thousand times smaller than the tens-of-nanometers change in the outer segment length we observed.

Thus, the observed deformations are assumed to be linked to the underlying electrical and physiological activity in photoreceptors and have accordingly been termed the optoretinogram, analogous to the electroretinogram. The slow expansion has been attributed to water influx due to the osmolytes produced in the phototransduction cascade (5,13), whereas we attribute the fast contractile response to the electromechanical consequences of the early receptor potential (ERP). The slow expansion has been used to classify cone types in vivo (4).

Compared with the point-scan and full-field optical coherence tomography (OCT) systems used in the past (5,15), a line-scan system captures an entire b-scan in each frame of the camera and thereby achieves sub-millisecond time resolution while recording structural information sufficient for the image registration. This is achieved by recording the spatial and spectral components of a b-scan across the x and y axes of a two-dimensional imager (11). The line-scan pOCT system applied here uses a superluminescent diode (λ = 840 nm, $\Delta\lambda$ = 50 nm) for the OCT path and a light emitting diode (LED) at 528 $\pm$ 20 nm for retinal stimulation. For high resolution measurements of the early response, it achieves an imaging field of $2 \times 0.6°$ on the retina, 5–7° temporal to the fovea, at a volume rate of 324 Hz. The early response recordings were captured at a b-scan rate of 16.2 kHz, and two B-scans were averaged to enable a temporal resolution of 123 μs. System sensitivity was 92 dB with phase sensitivity of 4 mrad at 50 dB signal-to-noise ratio (SNR), where 1 mrad $\approx$ 0.07 nm at λ_0 = 840 nm. The system attained speeds sufficient for revealing the details of the fast response in the cone outer segments, which were experimentally measured as a 5–40 nm contraction over less than 5 ms, preceding the slow swelling response.

The derivation of the physical model in Eq. 12 is detailed in the Supporting Materials and Methods. Results from the model were numerically integrated using the Runge-Kutta embedding technique with formulae of orders 4 and 5 {RK5(4)} (16) via the solve_ivp function in SciPy (17). Likewise, the parameters in the model were fitted to the data using a nonlinear least-squares optimization via the curve_fit function in SciPy.

RESULTS

Photon absorbed in the photoreceptor outer segment triggers several electrical and chemical changes as a part of the phototransduction cascade in photoreceptors. We are interested primarily in the first few milliseconds immediately after a photon absorption in an opsin embedded in the disk membrane and the resulting axial contraction that has been observed. There are two immediate effects to consider: 1) the direct conformational change of the opsin and a possible corresponding disk membrane area change and 2) the electrical potential induced by this same conformational

change and the corresponding change in forces due to the repulsion of ions in the Debye layer of the disk membrane.

Disk membrane area changes with conformational change

In the first case, crystallography and modeling studies predict the minute changes in the conformation of the embedded opsin during photoisomerization. This conformation change is the basis for the binding of G protein to the surface, which, in turn, enables the continuation of the phototransduction cascade. The change has been shown to feature a distinct outward tilt of the TM6 helix, moving by ~0.6 nm. Based on the models described in Park et al. (18), this 0.6 nm tilt is the predominant part of the conformational change. Given that the diameter of the TM6 helix is also ~0.6 nm, then a conservative estimate would be to assume the entire shift of this helix accounts for the area increase of the opsin as follows:

$$A_{add} = \pi(0.6/2)^2 = 0.28\,\mathrm{nm}^2. \quad (1)$$

This may be an overestimate of the area change because this does not account for the reorganization of lipids around the tilting helix or for the smaller (0.2 nm) shift of the TM5 helix toward the TM6 helix, which may itself decrease the area of the opsin. Given a 15% bleach of roughly 10^5 embedded opsins in a disk membrane, the relative area change in a 3.8 μm radius disk (and the corresponding relative axial change, per Eq. 7) would be $dz/z = -9.3 \times 10^{-5}$. This is 43 times smaller than the observed effect, as well as the voltage-dependent membrane tension effect we describe ($dz/z = -4 \times 10^{-3}$). In addition, because this conformational change per molecule does not depend on light intensity, it cannot account for the logarithmic saturation of the axial contraction with increasing brightness of the stimuli. Therefore, we neglect this minute effect in our model and focus instead on the electrical effect of the photoisomerization: the forces generated because of the membrane potential change.

ERP

The ERP is a millisecond-fast electrical signal after a bright stimulus, which has been observed in cone photoceptors via intracellular recordings or patch clamp (1,2,19). The ERP is attributed to charge transfer across the cell membrane that occurs during the photoisomerization of opsins (20,21). The origin of this charge transfer is complex, and the exact details of the conformational changes that lead to the charge transfer are not yet completely established. Suggested contributions to this effect include displacement of bound charges in the protein, change in dipole orientation, and charge migration (22).

Regardless of the exact structural details of the conformational change that leads to the ERP, the resulting potential change is well characterized and modeled (2,23). This ERP signal is distinct from the late receptor potential (LRP), which corresponds to changes in the cell potential associated with closing of the ion channels in outer segments as a consequence of the phototransduction cascade (1,2). As illustrated in Fig. 2, the change from 11 *cis*- to all-*trans* conformation of the opsin during isomerization results in a net shift of charge corresponding to a 10^{-10} V change in the membrane potential per photoisomerization. With an increasing number of incident photons, the ERP first increases linearly but then asymptotically (exponentially) reaches the saturation level as the 10^8 opsin molecules in the outer segment are increasingly bleached, reaching a saturated ERP level of U = −14.3 mV (2).

As opposed to the small increase in the footprint of the opsin during the conformational change, these millivolt changes in the membrane potential exert significant forces on the membrane. The transmembrane potential changes due to movement of ions across the cell membrane affect the charge density in the layers of mobile ions along the inner and outer surfaces of the membrane. Change in the lateral repulsion of these ions, in turn, affects the membrane tension, and the cell must rebalance the forces via a deformation. As we show, the resulting deformations can be very significant and can explain the observed behavior of the outer segments.

Voltage-dependent membrane tension

Rapid cellular deformations accompanying the changes in the transmembrane potential have been observed in multiple cell types, including the recent full-field interferometric imaging of human embryonic kidney (HEK) cells and neurons in cultuokre (7–10,24). These measurements have established a linear relationship between the membrane displacement and changes in cell potential, which are linked by the dependence of the membrane tension on transmembrane voltage.

The shape of biological cells is determined by the balance of intracellular hydrostatic pressure, membrane tension, and strain exerted by the cytoskeleton (25). The membrane tension includes a contractile component from the lipid bilayer and the lateral repulsion of ions in the Debye layer on both the intracellular and extracellular sides of the membrane:

$$T_{membrane} = \tau_{bilayer} + \tau_{ions} = \tau_{bilayer} - |\tau_{ions}|. \quad (2)$$

The lateral repulsion of ions can be expressed as a function of the charge density σ and ionic strength n on the inside, *in*, and outside, *ex*, of the membrane, as well as the transmembrane voltage V (7):

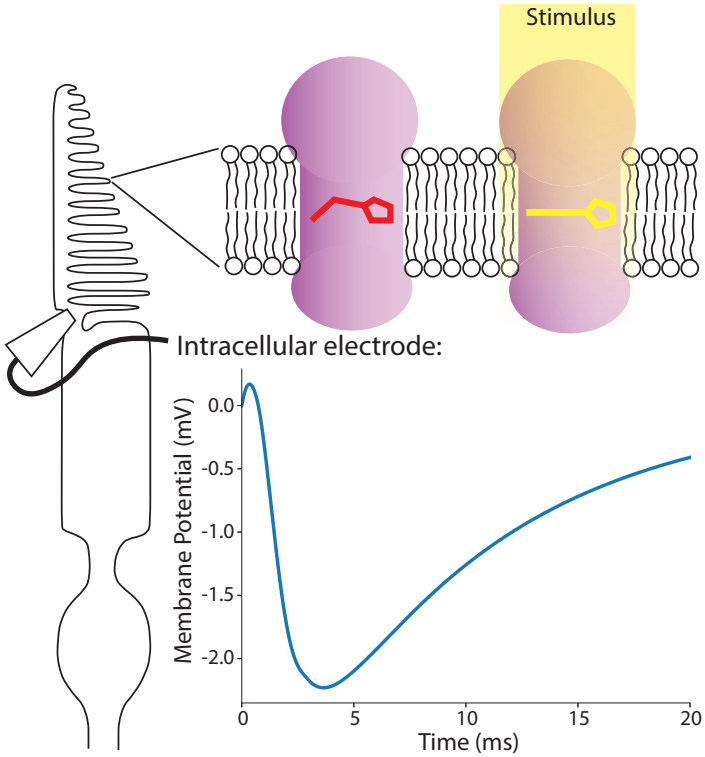

FIGURE 2 Intracellular electrical recording of the cone outer segment demonstrates the transmembrane potential transient after a 1 ms flash caused by the conformation change of the opsins embedded in the disk membranes. Each photoisomerization induces a 10^{-10} V potential change, leading to a characteristic potential change up to a few mV in the outer segment, with its time course shaped by the time constants of the various steps in the phototransduction cycle. To see this figure in color, go online.

$$T_{membrane} = \tau_{bilayer} - \frac{\sqrt{(2k_BT)^3\epsilon_w\epsilon_0}}{ze_0} \times \left(\sqrt{n_{ex}}\left[\sinh^{-1}\left\{\frac{\sigma_{ex} - C_mV}{2\sqrt{n_{ex}\epsilon_w\epsilon_0 2k_BT}}\right\}\right]^2 + \sqrt{n_{in}}\left[\sinh^{-1}\left\{\frac{\sigma_{in} + C_mV}{2\sqrt{n_{in}\epsilon_w\epsilon_0 2k_BT}}\right\}\right]^2\right). \quad (3)$$

Here, k_B is Boltzmann's constant, and T is the absolute temperature; ϵ_w and ϵ_0 are the relative permeability of water and the permittivity of free space, z is the number of valence ions in the solution, e_0 is the electronic charge, and C_m is the capacitance of the membrane between the Debye layers. The membrane tension increases by ~0.1 mN/m/V or 10 μN/ m^{-1} for a 100 mV depolarization (8). Increased surface tension of the cell membrane leads to deformation of a cell toward minimization of its surface area (i.e., becoming more spherical, which would be the case during the action potential (10)).

Quasistatic model

During hyperpolarization of the photoreceptor under illumination (the ERP), the lateral repulsion of ions τ_{ions} in the charge layers increases, and hence, the disk membrane area will expand. If the disk volume remains constant for a few milliseconds after the flash, widening of the disks will flatten them, leading to shortening of the outer segments, as illustrated in Fig. 3.

The disk membranes in photoreceptor outer segments have very low tension because they are formed as part of a blebbing process and contain no actin cortex (26–28). Because of this lack of structure, they lie flat in stacks that are held together by interdisk proteins (29). The low tension allows the membrane to undulate because of thermal fluctuations (30), and even small forces can easily pull the undulations out, leading to lateral expansion of the membrane, as shown in Fig. 4 *a*. The membrane area expansion coefficient at low tension is defined by the bending modulus $\kappa_c = 0.5 \times 10^{-19}$ N • m (30,31), whereas at high tension, when the undulations are flattened out, the area expansion modulus of a flat membrane $K_A = 0.2$ N/m dominates (32). The apparent modulus between these two extremes varies as a function of tension $\tilde{\tau}$ (33):

$$\frac{K}{K_A} = \left(1 + \frac{K_A k_B T}{8\pi\kappa_c\tilde{\tau}}\right)^{-1}. \quad (4)$$

At low tensions, K scales approximately linearly with $\tilde{\tau}$:

$$K \approx \frac{8\pi\kappa_c\tilde{\tau}}{k_BT}. \quad (5)$$

The range relevant for the physiological conditions of the disk membrane is very narrow and therefore linear, as indicated by the red arrow in Fig. 4 *b*. This linear relationship

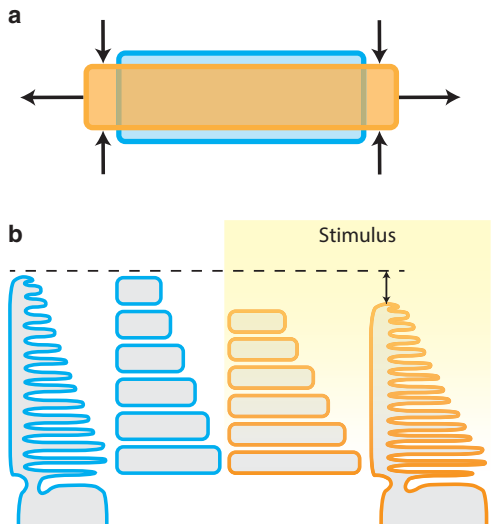

FIGURE 3 The deformation model of the photoreceptor outer segments assumes (*a*) the membrane expansion and subsequent flattening of the fixed-volume disks after the stimulus, which result in (*b*) the shrinkage of the outer segment that contains a stack of approximately 1000 disks. To see this figure in color, go online.

between the area expansion modulus and tension suggests a logarithmic relationship between the integrated expansion and applied tension in that range of interest. Following this intuition and based on the thermodynamic equilibrium considerations, Marsh (33) derives the normalized area expansion of a lipid membrane as

$$\frac{\Delta A}{A_0} = \frac{\tilde{\tau}}{K_A} + \frac{k_B T}{8\pi\kappa_c} \ln\left(\frac{\tilde{\tau}A/\pi^2\kappa_c + 1}{\tilde{\tau}a_1/\pi^2\kappa_c + 1}\right), \tag{6}$$

where A is the size of the membrane patch (in this case the area of the photoreceptor disk face with a radius around 3.5 μm (34)), A_0 is the area at zero observable tension $\tilde{\tau}$, and a_1 is the smallest bending feature size (area of a lipid head in a simple lipid bilayer membrane). In the case of a membrane densely filled with opsins (typically making up 50% of the membrane area), a_1 is likely not limited by the lipid head width, but rather by the characteristic size of the opsin nanodomains embedded in the disk membrane, which are ~25 nm in size (35). Fig. 4 *c* illustrates the saturation behavior of the area expansion with increasing tension for different values of a_1.

Considering a fixed volume of the disk as a cylinder $V = A \times z$, the change in thickness of the disk $\Delta z/z$ to accommodate this area expansion is

$$\frac{\Delta z}{z} = -\frac{\Delta A}{A}. \tag{7}$$

Because of the double pass of light reflected at the bottom of the outer segment, the corresponding change of the OPL is a function of its total height and the index of refraction:

$$OPL = \frac{\Delta z}{z} \times 2 \times \text{height} \times n_{index}. \tag{8}$$

With light intensities well below saturation of absorption (<15% bleaching of the opsins), the membrane potential change in the disk does not exceed a few millivolts and scales approximately linearly with the number of photons. This corresponds to ~ 0.01 nm OPL decrease per disk, but in an outer segment of 30 μm in height, made up of a stack of about 1000 disks, the overall deformation is in the tens of nanometers (Fig. 3).

As mentioned earlier, the membrane tension increases with the transmembrane voltage by 0.1 mN/m/V. Driving this tension change with the known time course of the ERP (Fig. 2; (2)), we can calculate the area expansion over time for this quasistatic model. To account for the slow swelling attributed to osmotic changes during phototransduction, as well as any tension change from the LRP, we also include a term linearly increasing with time

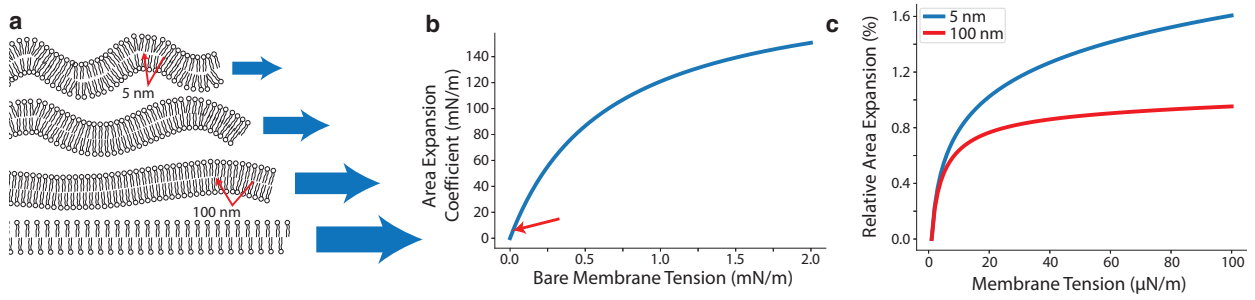

FIGURE 4 Saturation of the deformations due to the increasing expansion modulus of the disk membranes. (*a*) At low tensions, the disk membranes contain thermally induced fluctuations that require little force to pull out, depending on the smallest bending radius as labeled, but at higher forces, the intermolecular bonds of the membrane begin to dominate. (*b*) The resulting area expansion coefficient increases with tension, and in the small range of tensions relevant to the outer segment disks, indicated by the red arrow, can be approximated as a linear function of tension. (*c*) The relative area expansion thus saturates logarithmically over a 100-μN/m tension change. The rate of saturation depends on mechanical parameters of the membrane, notably including the minimal bending radius illustrated here, where 5 nm is the size of an individual lipid head. The larger minimal radii could be defined by the much larger opsins embedded in the membrane. To see this figure in color, go online.

(13,36). As shown in Fig. S2, this quasistatic model provides a poor fit to OPL changes measured in the living human eye. Most notably, this model does not allow for the variation of the time to peak with stimulus intensity, whereas observations show the negative peak shifts later in time with less intense stimuli (Fig. S2 *a*). However, the amplitude of the deformation is close to the observations with reasonable physical parameters, as summarized in Table 1, implying that the general basis of the model is sound.

Time-dependent model

To achieve a complete fit to the OPL changes over time, we must consider the dynamics of the disk membrane. Because the membrane stiffness K increases with tension, we expect it to behave as a nonlinear spring (Fig. S3). This could account for both the saturation of the peak amplitude and the faster time to peak with stronger stimuli. Assuming a linear scaling of the area expansion coefficient with tension in the range of interest (Fig. 4 *b*), the membrane can be modeled as a spring with a stiffness linearly increasing with the applied force and an offset

$$\frac{dF}{dx} = k(F(x)/N_0 + 1), \tag{9}$$

where k, analogous to a spring constant, will be fitted to the data, and N_0 is a dimensional unit of 1 N. The restoring force is then an exponential function of the displacement $F(x) = N_0(e^{kx} - 1)$, and deformation scales logarithmically with the applied force $x \propto 1\mathrm{n}(1 + F(x)/N_0)$, which is analogous to the scaling of the area expansion of the lipid membrane with tension (33)

$$\frac{\Delta A}{A_0} \propto \frac{1}{\alpha}\ln(1 + \tau/\beta), \tag{10}$$

where $\alpha = 8\pi\kappa_c/k_BT$ and $\beta = \pi^2\kappa_c/A_0$. Adding a velocity-dependent viscosity term, the membrane dynamics can be described as follows:

$$m\ddot{x} + c\dot{x} + N_0\left(e^{kx} - 1\right) = F(\text{photons}) = \tau(\text{photons}) \times l. \tag{11}$$

Fitting the parameters (m, c, k, and l) to the data yields a good match to both the amplitude and the time course of the deformation at different stimulus intensities. In the parameters that give the best fit, we see that $2\sqrt{mk} \ll c$, meaning the system is overdamped, and the mass term m is negligible. This corresponds to the low inertia of the disk membrane compared with the linear damping and restoring forces acting on it. With this simplification, the parameters in Eq. 11 can be derived from (33) to relate the deformation model to the underlying physical properties of the membrane (see Supporting Materials and Methods):

$$\frac{\eta r_0^2}{4}\dot{x} + \beta\left(e^{2\alpha x} - 1\right) = \tau(\text{photons}). \tag{12}$$

When fitted to the data, this model yields a damping coefficient $\eta = 6.7 \times 10^3$ kg m^{-2} s^{-1}, which is equivalent to the linear damping behavior due to the viscosity of a 100-nm sheet of water, not far from the tens-of-nanometers disk structures in photoreceptor outer segments. The other model parameters include a bending modulus $\kappa_c = 0.51 \times 10^{-19}$ N-m and a disk radius $r_0 = 3.8$ μm. This bending modulus and disk radius are typical for lipid membranes and cones at 5–7° temporal from the fovea (as in these measurements), respectively (34). Fig. 5 *a* shows the contributions from the fast response (ERP) and the linear slow response originating in the LRP and osmotic influx of water. The time course of the OPL changes recorded at two stimulus intensities were used to fit the parameters in Fig. 5 *b*, with the peak timing now properly accounted for. The same fitted parameters were then used to calculate the peak displacement across multiple stimulus intensities, and the resulting dependence matches well with the experimental observations, as shown in Fig. 5 *c*.

TABLE 1 Quasistatic Model Parameters

Parameter	Fit	Typical
Slow response slope	1.8×10^{-6} m/s	1×10^{-6} m/s
Initial tension	0.2 μN/m	0.1–1 μN/m
Bending modulus	2×10^{-19} N - m	$0.5–2 \times 10^{-19}$ N -m
Tension/voltage	−0.9 mN/m/V	−0.1 mN/m/V
Smallest patch size	10 nm	25 nm
Disk radius	3 μm	1–4 μm

DISCUSSION

The slow response modeled here as a linear function of time (Fig. 5) accounts for two effects: the voltage-dependent tension change resulting in membrane expansion due to the LRP, which begins ~4 ms after the stimulus (2), and the much larger and longer-lasting onset of the osmotic swelling (13). Both effects, separately, could contribute useful diagnostic insights into photoreceptor function and retinal health. The phototransduction cascade and the timing of its various stages is well studied (37), so the magnitude and dynamics of the swelling can be compared with these processes. Zhang et al. (13) suggest that the G protein complex disassociating from the disk membrane after photoisomerization and releasing into the cytoplasm could account for part of the osmotic misbalance and the associated influx of water into the outer segment. Comparison of the expected swelling from G protein with observations indicates that other osmolytes seem to contribute to this process as well (11).

A strong ERP signal has only been observed in intracellular recordings of cones, whose disks are continuous with

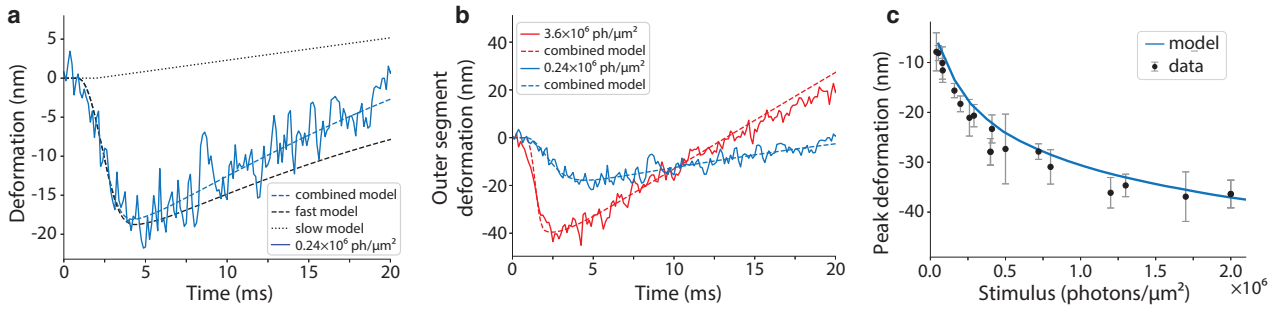

FIGURE 5 The time-dependent deformation model fits the observations well. (*a*) The combined model is comprised of two components: the fast contraction caused by the ERP and the linearly rising slow expansion that represents both the LRP and the osmotic swelling of the outer segment. (*b*) The model parameters are fitted to observations at two stimulus intensities; then the same parameters are used in (*c*) to predict the peak deformation as a function of stimulus intensity from additional measurements. The error bars denote +/- 1 standard deviation from 4 repeat measurements. To see this figure in color, go online.

the outer segment membrane, and hence the transmembrane potential is accessible to the probe patching the cilium (1,2). In rod photoreceptors, however, most of the disk membranes are pinched off and stacked within the outer segment membrane. Because the ERP is associated with the translocation of opsins across the disk membranes, very little potential change occurs across the outer segment membrane that the electrode has access to in rods. The small signal visible in such measurements is attributed to the minority of rhodopsin embedded in the outer segment membrane, as well as the few emerging disks at the base of the outer segment that have yet to pinch off (26–28). However, optical measurements of the fast response, in which mechanical deformations in each independent disk add up, should allow measurement of the ERP in rods without the limitations of electrical recordings. Based on preliminary measurements of deformations, as well as electrical measurements of the ERP in rods, we expect the deformation response in rods to be similar to the one that has been modeled and observed here in cones. The time course and amplitude of the variations are expected to be the same order of magnitude. Any variations in the conformational change of different opsins and the resulting potential changes of interest can be captured by the parametric nature of this model by adding terms to describe the progression of the ERP over time. In this study, the time course of the ERP was fixed to the model described by (2) from measurements of cone photoreceptors to match our experiment with the line-scan OCT system, but other opsins may require a specific model to capture their unique response.

Characterization of the nanometer-scale deformations in other electrically active cells, such as human embryonic kidney cells and cortical neurons, has benefited from a thorough understanding of the underlying mechanisms relating the membrane potential change to mechanical deformation (8,10). Cellular responses averaged over many trials provide a template for match-filtering temporal signals, thereby significantly boosting the detection performance. Likewise, comprehensive mechanical models of the cellular deformations due to the voltage-induced tension change provide a basis to interpret and refine the retinal recordings, including template matching for robust detection of such weak signals.

CONCLUSIONS

Interferometric recordings of the electrical activity in cells provide a noninvasive and label-free alternative for physiological characterization at single-cell resolution in vivo. Optoretinography has the potential to replace electroretinography, given the significant improvement in spatial resolution and signal specificity and the ability to provide co-registered structural and functional characterization of the retina. Our model of the fast contraction of the outer segment after light stimulus matches the experimental observations. The fast response is driven by the ERP, which is coupled to mechanical movement via the voltage-dependent membrane tension, leading to lateral expansion and axial contraction of the disks until the water influx takes over. The disk membrane's very soft, undulating initial state allows significant expansion until the membrane begins to flatten and becomes more resistant to further deformation. This leads to a logarithmic saturation of the amplitude and earlier arrival of the peak deformation with increasingly bright stimuli. Combination of this model with an accurate description of the slower phases originating in the LRP and osmotic swelling can be used in the future to characterize various aspects of the photoreceptor physiology in health and disease.

SUPPORTING MATERIAL

Supporting Material can be found online at https://doi.org/10.1016/j.bpj.2020.09.005.

AUTHOR CONTRIBUTIONS

K.C.B. and T.L. applied the deformation model to photoreceptor measurements. K.C.B. and Z.C.C. developed the analytical model based on

underlying physical parameters. D.P. supervised the work. V.P.P., J.K., and R.S. captured the data. K.C.B., Z.C.C., and D.P. wrote the manuscript.

ACKNOWLEDGMENTS

We thank Dr. Denis Baylor for very helpful discussions about photoreceptors and the ERP and Dr. Lenya Ryzhik for input on the modeling of the disk deformations. V.P.P., R.S., and D.P. have a provisional US patent describing optoretinography.

Funding was provided by National Institutes of Health Grants U01 EY025501, R21EY027941, R01EY029710, P30EY001730, and an unrestricted grant from Research to Prevent Blindness, a Research to Prevent Blindness Career Development Award, the Burroughs Welcome Fund Careers at the Scientific Interfaces, and the Murdock Charitable Trust.

REFERENCES

1. Müller, W., and H. Töpke. 1987. The early receptor potential (ERP). *Doc. Ophthalmol.* 66:35–74.
2. Hodgkin, A. L., and P. M. Obryan. 1977. Internal recording of the early receptor potential in turtle cones. *J. Physiol.* 267:737–766.
3. Smith, N. P., and T. D. Lamb. 1997. The a-wave of the human electroretinogram recorded with a minimally invasive technique. *Vision Res.* 37:2943–2952.
4. Zhang, F., K. Kurokawa, …, D. T. Miller. 2019. Cone photoreceptor classification in the living human eye from photostimulation-induced phase dynamics. *Proc. Natl. Acad. Sci. USA.* 116:7951–7956.
5. Hillmann, D., H. Spahr, …, G. Hüttmann. 2016. In vivo optical imaging of physiological responses to photostimulation in human photoreceptors. *Proc. Natl. Acad. Sci. USA.* 113:13138–13143.
6. Liu, Z., K. Kurokawa, …, D. T. Miller. 2017. Imaging and quantifying ganglion cells and other transparent neurons in the living human retina. *Proc. Natl. Acad. Sci. USA.* 114:12803–12808.
7. Zhang, P. C., A. M. Keleshian, and F. Sachs. 2001. Voltage-induced membrane movement. *Nature.* 413:428–432.
8. Ling, T., K. C. Boyle, …, D. Palanker. 2018. Full-field interferometric imaging of propagating action potentials. *Light Sci. Appl.* 7:107.
9. Kim, G. H., P. Kosterin, …, B. M. Salzberg. 2007. A mechanical spike accompanies the action potential in Mammalian nerve terminals. *Biophys. J.* 92:3122–3129.
10. Ling, T., K. C. Boyle, …, D. Palanker. 2020. High-speed interferometric imaging reveals dynamics of neuronal deformation during the action potential. *Proc. Natl. Acad. Sci. USA.* 117:10278–10285.
11. Pandiyan, V. P., A. M. Bertelli, J. A. Kuchenbecker, K. C. Boyle, T. Ling, Z. C. Chen, B. H. Park, A. Roorda, D. Palanker, and R. Sabesan. 2020. The optoretinogram reveals the primary steps of phototransduction in the living human eye. *Sci. Adv.* 6:eabc1124.
12. Pandiyan, V. P., X. Jiang, A. Maloney-Bertelli, J. A. Kuchenbecker, U. Sharma, and R. Sabesan. 2020. High-speed adaptive optics line-scan OCT for cellular-resolution optoretinography. *Bio. Opt. Exp.* 11:5274–5296.
13. Zhang, P., R. J. Zawadzki, …, E. N. Pugh, Jr. 2017. In vivo optophysiology reveals that G-protein activation triggers osmotic swelling and increased light scattering of rod photoreceptors. *Proc. Natl. Acad. Sci. USA.* 114:E2937–E2946.
14. Goetz, G., T. Ling, …, D. Palanker. 2018. Interferometric mapping of material properties using thermal perturbation. *Proc. Natl. Acad. Sci. USA.* 115:E2499–E2508.
15. Azimipour, M., J. V. Migacz, …, R. S. Jonnal. 2019. Functional retinal imaging using adaptive optics swept-source OCT at 1.6 MHz. *Optica.* 6:300–303.
16. Dormand, J. R., and P. J. Prince. 1980. A family of embedded Runge-Kutta formulae. *J. Comput. Appl. Math.* 6:19–26.
17. Virtanen, P., R. Gommers, …, P. van Mulbregt; SciPy 1.0 Contributors. 2020. SciPy 1.0: fundamental algorithms for scientific computing in Python. *Nat. Methods.* 17:261–272.
18. Park, J. H., P. Scheerer, …, O. P. Ernst. 2008. Crystal structure of the ligand-free G-protein-coupled receptor opsin. *Nature.* 454:183–187.
19. Brown, K. T., and M. Murakami. 1964. A new receptor potential of the monkey retina with no detectable latency. *Nature.* 201:626–628.
20. Sullivan, J. M., and P. Shukla. 1999. Time-resolved rhodopsin activation currents in a unicellular expression system. *Biophys. J.* 77:1333–1357.
21. Sakmar, T. P. 1999. Rhodopsin early receptor potential revisited. *Biophys. J.* 77:1189–1191.
22. Honig, B. H., W. L. Hubbell, and R. F. Flewelling. 1986. Electrostatic interactions in membranes and proteins. *Annu. Rev. Biophys. Biophys. Chem.* 15:163–193.
23. Makino, C. L., W. R. Taylor, and D. A. Baylor. 1991. Rapid charge movements and photosensitivity of visual pigments in salamander rods and cones. *J. Physiol.* 442:761–780.
24. Oh, S., C. Fang-Yen, …, M. S. Feld. 2012. Label-free imaging of membrane potential using membrane electromotility. *Biophys. J.* 103:11–18.
25. Diz-Muñoz, A., D. A. Fletcher, and O. D. Weiner. 2013. Use the force: membrane tension as an organizer of cell shape and motility. *Trends Cell Biol.* 23:47–53.
26. Volland, S., L. C. Hughes, …, D. S. Williams. 2015. Three-dimensional organization of nascent rod outer segment disk membranes. *Proc. Natl. Acad. Sci. USA.* 112:14870–14875.
27. Burgoyne, T., I. P. Meschede, …, C. E. Futter. 2015. Rod disc renewal occurs by evagination of the ciliary plasma membrane that makes cadherin-based contacts with the inner segment. *Proc. Natl. Acad. Sci. USA.* 112:15922–15927.
28. Dai, J., and M. P. Sheetz. 1999. Membrane tether formation from blebbing cells. *Biophys. J.* 77:3363–3370.
29. Goldberg, A. F. X., O. L. Moritz, and D. S. Williams. 2016. Molecular basis for photoreceptor outer segment architecture. *Prog. Retin. Eye Res.* 55:52–81.
30. Evans, E., and W. Rawicz. 1990. Entropy-driven tension and bending elasticity in condensed-fluid membranes. *Phys. Rev. Lett.* 64:2094–2097.
31. Helfrich, W., and R. M. Servuss. 1984. Undulations, steric interaction and cohesion of fluid membranes. *Il Nuovo Cimento D.* 3:137–151.
32. Phillips, R. 2018. Membranes by the numbers. *In* Physics of Biological Membranes. P. Bassereau and P. Sens, eds. Springer International Publishing, pp. 73–105.
33. Marsh, D. 1997. Renormalization of the tension and area expansion modulus in fluid membranes. *Biophys. J.* 73:865–869.
34. Curcio, C. A., K. R. Sloan, …, A. E. Hendrickson. 1990. Human photoreceptor topography. *J. Comp. Neurol.* 292:497–523.
35. Rakshit, T., S. Senapati, …, P. S.-H. Park. 2015. Rhodopsin forms nanodomains in rod outer segment disc membranes of the cold-blooded xenopus laevis. *PLoS One.* 10:e0141114.
36. Lu, Y., J. Benedetti, and X. Yao. 2018. Light-induced length shrinkage of rod photoreceptor outer segments. *Transl. Vis. Sci. Technol.* 7:29.
37. Korenbrot, J. I. 2012. Speed, sensitivity, and stability of the light response in rod and cone photoreceptors: facts and models. *Prog. Retin. Eye Res.* 31:442–466.